Available online at www.sciencedirect.com
SCIENCE DIRECT®
Materials Research Bulletin 40 (2005) 682–693
Materials Research Bulletin
www.elsevier.com/locate/matresbu

Structural features of $AgCaCdMg_2(PO_4)_3$ and $AgCd_2Mg_2(PO_4)_3$, two new compounds with the alluaudite-type structure, and their catalytic activity in butan-2-ol conversion

Mohammed Kacimi[a], Mahfoud Ziyad[a], Frédéric Hatert[b,*]

[a]*Faculté des Sciences, Laboratoire de Physico-Chimie des Matériaux et Catalyse, Département de Chimie, Avenue Ibn Battouta, Rabat, Morocco*
[b]*Laboratoire de Minéralogie, Université de Liège, B18, B-4000 Liège, Belgium*

Received 10 May 2004; received in revised form 16 November 2004; accepted 31 December 2004

Abstract

$AgCaCdMg_2(PO_4)_3$ and $AgCd_2Mg_2(PO_4)_3$, two new compounds with the alluaudite-type structure, were synthesized by a solid state reaction in air at 750 °C. The X-ray powder diffraction pattern of $AgCaCdMg_2(PO_4)_3$ indicates the presence of small amounts of $(Ca, Mg)_3(PO_4)_2$ with the whitlockite structure, as impurity, whereas $AgCd_2Mg_2(PO_4)_3$ is constituted by pure alluaudite. The Rietveld refinements of the X-ray powder diffraction patterns indicate an ordered cationic distribution for $AgCd_2Mg_2(PO_4)_3$, with Ag on A(2)′, Cd on A(1) and M(1), and Mg on M(2), whereas a disordered distribution of Cd and Ca between the A(1) and M(1) sites is observed for $AgCaCdMg_2(PO_4)_3$. The catalytic properties of these compounds has been measured in reaction of butan-2-ol dehydrogenation. In the absence of oxygen, both samples exhibit poor dehydrogenation activity. All samples displayed no dehydration activity. Introduction of oxygen into the feed changed totally the catalytic behavior of the catalysts. The production of methyl ethyl ketone increases with time on stream and the reaction temperature. $AgCaCdMg_2(PO_4)_3$ is more efficient than $AgCd_2Mg_2(PO_4)_3$.

Keywords: D. Catalytic properties

* Corresponding author. Tel.: +32 43662143; fax: +32 43662202.
E-mail address: fhatert@ulg.ac.be (F. Hatert).

0025-5408/$ – see front matter © 2005 Elsevier Ltd. All rights reserved.
doi:10.1016/j.materresbull.2004.12.009

1. Introduction

Several phosphates have been recognized in recent years to have good catalytic activity in various reactions that require acid–base properties or redox sites [1,2]. In order to increase our knowledge on the catalysis by these materials we have studied several structural families of phosphates such as apatite, olivine and nasicon-type structures.

The nasicon phosphates of general formula $M_nM'_2(PO_4)_3$ ($M = Cu^+$, Ag^+, $M' = Zr^{4+}$, Hf^{4+}, $n = 0.5$, 1) exhibit a three-dimensional structure where $[PO_4]$ tetrahedra and $[M'O_6]$ octahedra delimit cavities that can host mono and divalent cations [3]. It was found that during a catalytic reaction, the monovalent cations can be reduced and diffuse to the material surface to form metallic particles. Concomitantly, protons conceded by reactants replace the reduced cations in the structure, in order to preserve the electric neutrality of the phosphate [3,4]. Similar observations and comparable activities have been recorded in the case of phosphates of general formula $MTh_2(PO_4)_3$ ($M = Cu^+$, Ag^+). The structural differences between these two families are probably best pictured by the nature and the morphology of the metallic aggregation formed while the catalyst is 'working'. In the case of nasicon-type phosphates, the aggregation leads to formation of filaments, whereas in the case of $MTh_2(PO_4)_3$ catalysts, the reduction produces particles with a size around 10 Å [5,6]. Other phosphates such as the whitlockite-type materials, with a general formula $Ca_{10.5-x}M_x(PO_4)_7$ (M = Cu, Fe), have also been studied. When $M = Cu^{2+}$, these compounds show a catalytic activity in butan-2-ol dehydrogenation that depended on the amount of copper substituted in the phosphate. Characterization of these compounds by spectroscopic techniques showed that the catalytic activity was attributed to the redox properties of Cu^{2+} ions hosted by Ca [4] sites [7,8]. These sites are of octahedral symmetry and localized in large cavities where the transition ions have a large mobility.

The alluaudite family of minerals consists of Na–Mn–Fe-bearing phosphates which are known to occur in granitic pegmatites. Moore [9] determined the crystal structure of alluaudite in the monoclinic system with *C2/c* space group and derived the general structural formula $X(2)X(1)M(1)M(2)_2(PO_4)_3$ ($Z = 4$). The structure consists of kinked chains of edge-sharing octahedra stacked parallel to {1 0 1}. These chains are formed by a succession of M(2) octahedral pairs linked by highly distorted M(1) octahedra. Equivalent chains are connected in the *b* direction by the P(1) and P(2) phosphate tetrahedra to form sheets oriented perpendicular to [0 1 0]. These interconnected sheets produce channels parallel to the *c* axis, channels which contain the distorted cubic X(1) site and the four-coordinated X(2) site.

The past decade has seen an increasing number of structural studies of synthetic phosphates with the alluaudite structure. The papers mentioned in the literature [11–13,15,17–30] clearly demonstrate the existence of three cationic sites in the alluaudite structure which were not reported by Moore [9]. These sites are located in the channels, on crystallographic positions which are different from those of X(1) and X(2). Based on detailed structural studies, Hatert et al. [23] proposed a new general formula, $[A(2)A(2)'][A(1)A(1)'A(1)''_2]M(1)M(2)_2[PO_4]_3$, for alluaudite-type compounds.

The existence of channels in the alluaudite structure makes possible its use as an ionic or electronic conductor. Warner et al. [11] synthesized $Cu_{1.35}Fe_3(PO_4)_3$ and $Cu_2Mg_3(PO_4)_3$, which contain mixed valences of Cu and Fe. Warner and Maier [12] showed that $Cu_2Mg_3(PO_4)_3$ exhibits a mixed Cu^+ ionic and electronic conductivity, whereas Daidouh et al. [26] gave evidence of the ionic character of the electronic conductivity of $(Ag_{1-x}Na_x)_2Mn_2Fe(PO_4)_3$.

The alluaudite-type structure shares similarities with garnet, langbeinite, nasicon and $Sc_2(WO_4)_3$ structures and might display analogous catalytic behaviour [10]. The present work is devoted to the investigation of the catalytic activity of some compounds belonging to this structure-type, such as

$AgCaCdMg_2(PO_4)_3$ and $AgCd_2Mg_2(PO_4)_3$. These newly synthesized compounds are also structurally characterized. Their catalytic performances will be studied and compared to that of other phosphates using butan-2-ol as the probe reaction. This reaction provides information on the acid–base and redox properties of catalysts, as well as on changes that the catalyst might undergo on stream [14].

2. Experimental

The catalysts have been prepared using a method analogous to that proposed by Antenucci et al. for the synthesis of $NaCaCdMg_2(PO_4)_3$ [15]. Stoichiometric quantities of Ag_2SO_4, $M(NO_3)_2$ (M = Ca, Cd, Mg) and $NH_4H_2PO_4$ were dissolved in HNO_3 (6 M). The resulting mixture was heated under stirring up to 85 °C until the complete evaporation of the solvent. The recovered solids were successively calcined at 300 (12 h), 500 (12 h), 600 (12 h) and finally at 750 °C (3× 48 h) with intermittent grindings at each temperature.

X-ray powder diffraction patterns of the compounds were recorded on a Philips PW-3710 diffractometer using the 1.9373 Å Fe Kα radiation. The unit-cell parameters were calculated with the least-squares refinement program LCLSQ 8.4 [31], from the *d*-spacings calibrated with $Pb(NO_3)_2$ as an internal standard. These unit-cell parameters, and the atomic positions reported for $NaCaCdMg_2(PO_4)_3$ [15], served as starting parameters for the Rietveld refinements which were performed with the DBWS-9807 program developed by Young et al. [32]. The investigated 2θ range extended from 10° to 100°, the step width was 0.02°, and the step time was 15 s. The total number of refined parameters was 50 and 53, with 509 and 510 observed reflections, for $AgCaCdMg_2(PO_4)_3$ and $AgCd_2Mg_2(PO_4)_3$, respectively. The final Rietveld plot for $AgCd_2Mg_2(PO_4)_3$ is shown in Fig. 1.

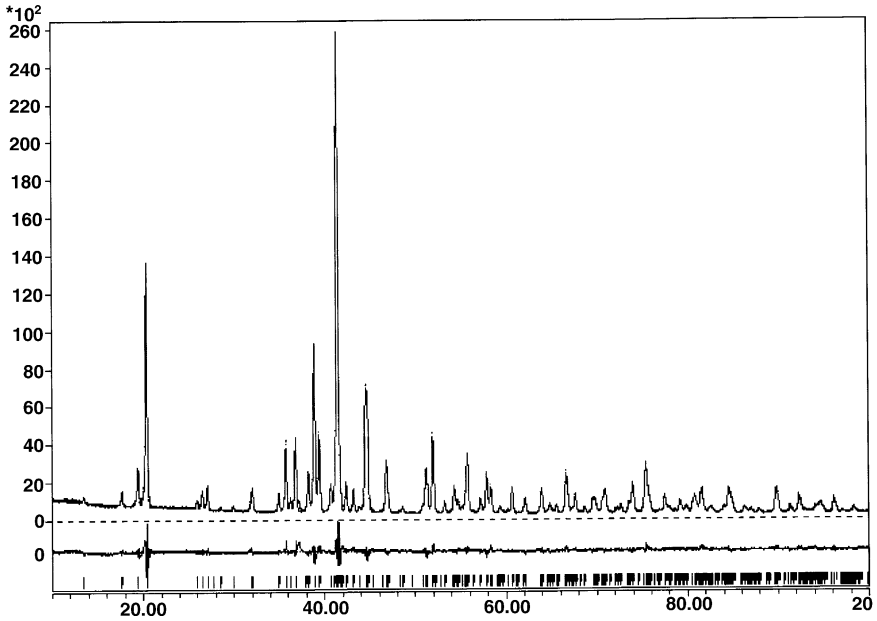

Fig. 1. The observed (dots), calculated (solid line), and difference X-ray powder diffraction patterns of $AgCd_2Mg_2(PO_4)_3$ obtained from a Rietveld refinement. The vertical markers indicate the positions calculated for the Fe $K\alpha_1$ and Fe $K\alpha_2$ Bragg reflections.

Infrared spectra were recorded with a Nicolet NEXUS spectrometer, from 50 scans with a 2 cm^{-1} resolution, over the 400–4000 cm^{-1} region. The samples were prepared by mixing intimately 2 mg of alluaudite-type compounds with KBr, in order to obtain a 150 mg homogeneous pellet which was dried for a few hours at 110 °C. To prevent water contamination, the measurements were performed under a dry-air purge.

The catalytic tests were carried out in U-shaped dynamic micro-reactor operating at atmospheric pressure. The catalyst was sieved to 120 μm and maintained in the reactor between two quartz wool plugs. The butan-2-ol was supplied to the reactor diluted in nitrogen or air at a partial pressure equal to 12.2×10^3 Pa and a total flow rate of 60 cm^3 min^{-1}. Prior to the reaction, 100 mg of the sample were evacuated for 2 h at 450 °C under a pure stream of N_2. Analysis of the reaction mixture was performed by on-line Varian 3600 chromatograph equipped with FID and catharometer detectors. The reaction products were identified and separated on 4 m (1/8 in.) stainless-steel columns packed with Carbowax 1500 (15%) on Chromosorb PAW (60/80 mesh) and Porapak Q. The catalyst activity was calculated in terms of percentages of butan-2-ol converted into butenes, methyl ethyl ketone and carbon dioxide when O_2 is added to the reaction mixture.

3. Results and discussion

3.1. Structural features

The X-ray powder diffraction pattern of $AgCaCdMg_2(PO_4)_3$ indicates the presence of small amounts of $(Ca, Mg)_3(PO_4)_2$ with the whitlockite structure, as impurity, whereas $AgCd_2Mg_2(PO_4)_3$ is constituted by pure alluaudite. The unit-cell parameters, reliability factors, positional parameters, site occupancies, and interatomic distances and angles, deduced from the Rietveld refinements, are given in Tables 1–3, respectively. Both the satisfactory values of R_p, R_{wp}, R_{Bragg}, and S (Table 1), and the mean O–P(1)–O and O–P(2)–O angles (Table 3), which are close to those of an ideal tetrahedron, confirm the reliability of the refinements. However, the reliability factors for $AgCd_2Mg_2(PO_4)_3$ are better that those of $AgCaCdMg_2(PO_4)_3$, probably because small amounts of impurities occur in the latter compound. A

Table 1
Unit-cell parameters and reliability factors for the alluaudite-type compounds, $AgCaCdMg_2(PO_4)_3$ and $AgCd_2Mg_2(PO_4)_3$

	$AgCaCdMg_2(PO_4)_3$	$AgCd_2Mg_2(PO_4)_3$
S.G.	*C*2/*c*	*C*2/*c*
a (Å)	12.106(3)	12.089(3)
b (Å)	12.677(2)	12.653(2)
c (Å)	6.525(1)	6.530(1)
β (°)	114.67(2)	114.71(2)
Volume (Å^3)	909.9(2)	907.4(2)
R_p (%)	7.19	6.41
R_{wp} (%)	9.32	8.36
$R_{exp.}$ (%)	3.39	3.29
S	2.73	2.53
$R_{(Bragg)}$ (%)	8.36	5.95

Table 2
Positional (x, y, z), isotropic thermal (B) and site occupancy (N) parameters for the synthetic alluaudite-type compounds, $AgCaCdMg_2(PO_4)_3$ and $AgCd_2Mg_2(PO_4)_3$

Site	Atom	Wyckoff	x	y	z	B (Å^2)	N
$AgCaCdMg_2(PO_4)_3$							
A(2)′	Ag	4*e*	0	−0.0186(3)	0.25	0.5	0.440(4)
A(1)	Cd	4*b*	0.50	0	0	0.5	0.314(5)
	Ca	4*b*	0.50	0	0	0.5	0.136(5)
	Ag	4*b*	0.50	0	0	0.5	0.05
M(1)	Ca	4*e*	0	0.2624(4)	0.25	0.5	0.257(5)
	Cd	4*e*	0	0.2624(4)	0.25	0.5	0.243(5)
M(2)	Mg	8*f*	0.2789(9)	0.6599(6)	0.368(2)	0.5	1.07(2)
P(1)	P	4*e*	0	−0.2836(9)	0.25	0.5	0.50
P(2)	P	8*f*	0.2414(8)	−0.0996(7)	0.135(2)	0.5	1.00
O(1)	O	8*f*	0.454(1)	0.709(1)	0.552(2)	1.0	1.00
O(2)	O	8*f*	0.098(1)	0.648(1)	0.227(2)	1.0	1.00
O(3)	O	8*f*	0.309(1)	0.657(1)	0.069(3)	1.0	1.00
O(4)	O	8*f*	0.122(1)	0.419(1)	0.316(2)	1.0	1.00
O(5)	O	8*f*	0.236(1)	0.818(1)	0.321(3)	1.0	1.00
O(6)	O	8*f*	0.324(1)	0.501(1)	0.401(2)	1.0	1.00
$AgCd_2Mg_2(PO_4)_3$							
A(2)′	Ag	4*e*	0	−0.0174(2)	0.25	0.5	0.480(3)
A(1)	Cd	4*b*	0.50	0	0	0.5	0.489(3)
M(1)	Cd	4*e*	0	0.2604(2)	0.25	0.5	0.503(3)
M(2)	Mg	8*f*	0.2775(6)	0.6600(4)	0.367(1)	0.5	1.17(1)
P(1)	P	4*e*	0	−0.2830(8)	0.25	0.5	0.50
P(2)	P	8*f*	0.2365(6)	−0.1022(5)	0.130(1)	0.5	1.00
O(1)	O	8*f*	0.455(1)	0.714(1)	0.552(2)	1.0	1.00
O(2)	O	8*f*	0.095(1)	0.6411(9)	0.224(2)	1.0	1.00
O(3)	O	8*f*	0.313(1)	0.657(1)	0.086(2)	1.0	1.00
O(4)	O	8*f*	0.129(1)	0.4123(9)	0.315(2)	1.0	1.00
O(5)	O	8*f*	0.232(1)	0.8197(9)	0.323(2)	1.0	1.00
O(6)	O	8*f*	0.3228(9)	0.496(1)	0.390(2)	1.0	1.00

polyhedral representation of the crystal structure of $AgCd_2Mg_2(PO_4)_3$, projected along the approximate [0 0 1] direction, is shown in Fig. 2.

The crystallographic sites of the alluaudite-like compounds (Table 2) are labeled according to the nomenclature recently proposed by Hatert et al. [23]. The morphologies of the coordination polyhedra of M(1) and M(2) are those of distorted octahedra, whereas the morphologies of A(1) and A(2)′ are those of a distorted cube and a gabled disphenoid, respectively. However, if the bond distances longer than 3.0 Å are neglected, the morphologies of A(1) and A(2)′ become those of a distorted octahedron and of a trigonal prism, respectively. These morphologies are similar to those previously described for $NaCaCdMg_2(PO_4)_3$ [15].

The temperature factors were not refined, because they are correlated with the occupancy factors. Consequently, the temperature factors were constrained to the reasonable values 0.5 (Ag, Ca, Cd, Mg, P) and 1.0 (O), which are close to the values obtained by Antenucci et al. [15] and Hatert et al. [23,24].

Preliminary refinements were performed assuming an ordered distribution of Ag, Ca, Cd, and Mg on the crystallographic sites of the alluaudite structure, according to the ionic radii of these cations. For

Table 3
Selected interatomic distances (Å) and angles (°) for the synthetic alluaudite-type compounds, $AgCaCdMg_2(PO_4)_3$ and $AgCd_2Mg_2(PO_4)_3$

	$AgCaCdMg_2(PO_4)_3$	$AgCd_2Mg_2(PO_4)_3$
A(2)′–O(6) × 2	2.39(1)	2.445(9)
A(2)′–O(6) × 2	2.709(9)	2.663(7)
A(2)′–O(1) × 2	2.69(1)	2.75(1)
A(2)′–O(3) × 2	3.07(1)	3.02(1)
Mean	2.71	2.72
A(1)–O(4) × 2	2.22(1)	2.28(1)
A(1)–O(2) × 2	2.37(1)	2.29(1)
A(1)–O(4) × 2	2.43(1)	2.588(9)
A(1)–O(2) × 2	3.14(1)	3.08(1)
Mean	2.54	2.56
M(1)–O(1) × 2	2.38(1)	2.33(1)
M(1)–O(4) × 2	2.41(1)	2.40(1)
M(1)–O(3) × 2	2.50(1)	2.44(1)
Mean	2.43	2.39
M(2)–O(2)	2.00(1)	2.02(1)
M(2)–O(6)	2.08(2)	2.14(2)
M(2)–O(1)	2.03(1)	2.09(1)
M(2)–O(5)	2.06(1)	2.08(1)
M(2)–O(3)	2.13(2)	2.05(1)
M(2)–O(5)	2.13(2)	2.09(1)
Mean	2.07	2.08
P(1)–O(1) × 2	1.51(2)	1.46(1)
P(1)–O(2) × 2	1.53(1)	1.56(1)
Mean	1.52	1.51
P(2)–O(3)	1.41(2)	1.46(1)
P(2)–O(6)	1.47(2)	1.41(2)
P(2)–O(4)	1.56(1)	1.523(9)
P(2)–O(5)	1.63(2)	1.62(1)
Mean	1.52	1.50
O(2)–P(1)–O(2)	110.4(9)	104.0(8)
O(1)–P(1)–O(1)	102.3(10)	106.8(9)
O(2)–P(1)–O(1) × 2	113.7(6)	116.4(5)
O(2)–P(1)–O(1) × 2	108.3(6)	106.9(5)
Mean	109.5	109.6
O(4)–P(2)–O(3)	105.9(7)	104.6(6)
O(6)–P(2)–O(3)	107.7(9)	110.0(7)
O(6)–P(2)–O(5)	119.5(7)	115.2(6)
O(5)–P(2)–O(3)	103.7(9)	109.2(7)
O(6)–P(2)–O(4)	110.8(9)	111.5(7)
O(4)–P(2)–O(5)	108.4(8)	105.8(6)
Mean	109.3	109.4

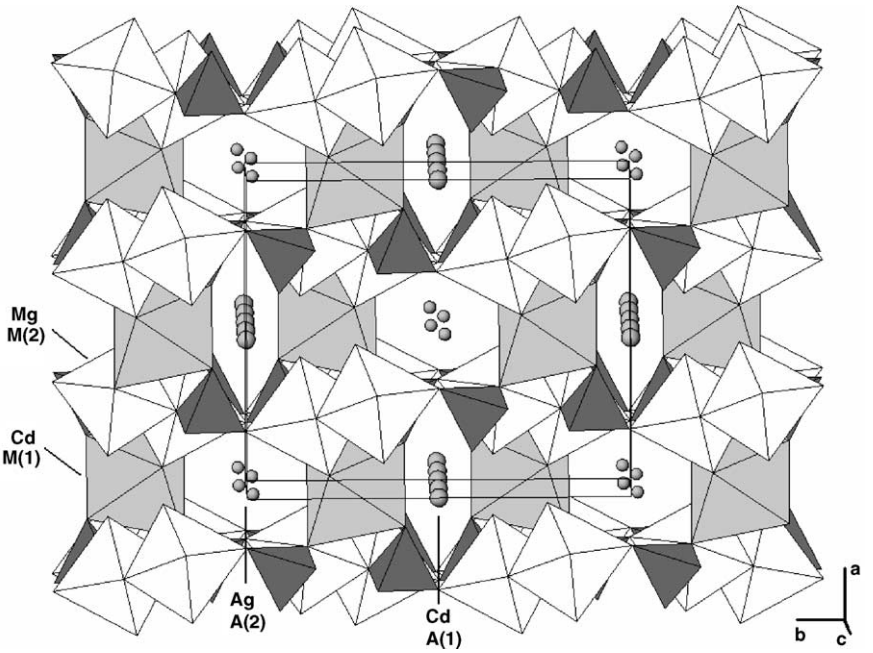

Fig. 2. The projection of the crystal structure of $AgCd_2Mg_2(PO_4)_3$. The PO_4 tetrahedra are densely shaded. The shaded M(1) octahedra are occupied by Cd, and the unshaded M(2) octahedra are occupied by Mg. The circles indicate Cd and Ag on the A(1) and A(2)′ crystallographic sites.

$AgCd_2Mg_2(PO_4)_3$, the final occupancy factors (Table 2) are in good agreement with this ordered distribution, with Ag on A(2)′, Cd on A(1) and M(1), and Mg on M(2). However, preliminary refinements of $AgCaCdMg_2(PO_4)_3$ indicate a rather low electronic density on M(1) and a high electronic density on A(1), compared to the theoretical values. This behavior is likely related to the presence of Ca on the M(1) site and of Cd on the A(1) site. Consequently, the occupancy factors for the A(1) and M(1) sites were calculated assuming a full occupancy by Ca and Cd.

Another problem arises from the presence of $(Ca, Mg)_3(PO_4)_2$ as impurity, which produces a lowering of the Ca-content of $AgCaCdMg_2(PO_4)_3$. For this reason, and because no vacancies were observed on the A(1) site, it was necessary to introduce a small amount of Ag on A(1). This amount, which was fixed to 10%, corresponds approximately to the deficit of Ag observed on the A(2)′ crystallographic site (Table 2). The final refinement was then performed assuming Ag and vacancies in A(2)′, Cd, Ca and Ag in A(1), Ca and Cd in M(1), and Mg in M(2). This partially disordered distribution of Ca and Cd between the A(1) and M(1) sites (Table 2) is probably due to the similar ionic radii of Ca^{2+} and Cd^{2+}, radii which are 1.00 and 0.95 Å, respectively [33]. A similar disordered distribution has already been observed by Antenucci et al. [15] in the alluaudite-like compound $NaCaCdMg_2(PO_4)_3$.

3.2. Infrared spectroscopy

The infrared spectra of $AgCaCdMg_2(PO_4)_3$ and $AgCd_2Mg_2(PO_4)_3$, shown in Fig. 3, are typical of an orthophosphate structure [34]. Because the infrared spectra of alluaudites exhibit a complexity which is related to the low symmetry and the large dimensions of the unit-cell [35], it is difficult to attribute all the

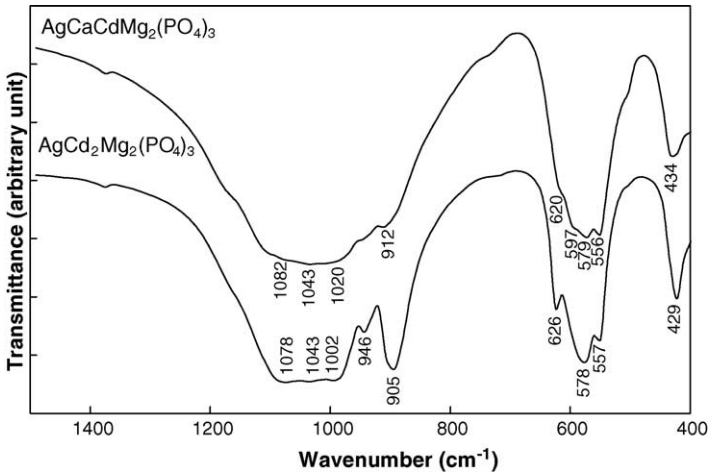

Fig. 3. The infrared spectra of the $AgCaCdMg_2(PO_4)_3$ and $AgCd_2Mg_2(PO_4)_3$ alluaudite-type compounds.

individual absorption bands to specific modes of vibration. Nevertheless, most of the bands can be assigned by comparison with the similar spectra of $NaCdIn_2(PO_4)_3$ and $NaMn(Fe_{1-x}In_x)_2(PO_4)_3$ [35,29]. According to these authors, the stretching vibrational modes of the PO_4 tetrahedra appear in the 1200–850 cm^{-1} region, whereas the PO_4 bending vibrational modes occur between ca. 400 and 650 cm^{-1}.

Qualitatively, sharp bands are observed for $AgCd_2Mg_2(PO_4)_3$, whereas broader bands are obtained with $AgCaCdMg_2(PO_4)_3$. This feature confirms the disordered distribution of Ag, Ca, and Cd in $AgCaCdMg_2(PO_4)_3$, whereas the cationic distribution in $AgCd_2Mg_2(PO_4)_3$ is more ordered.

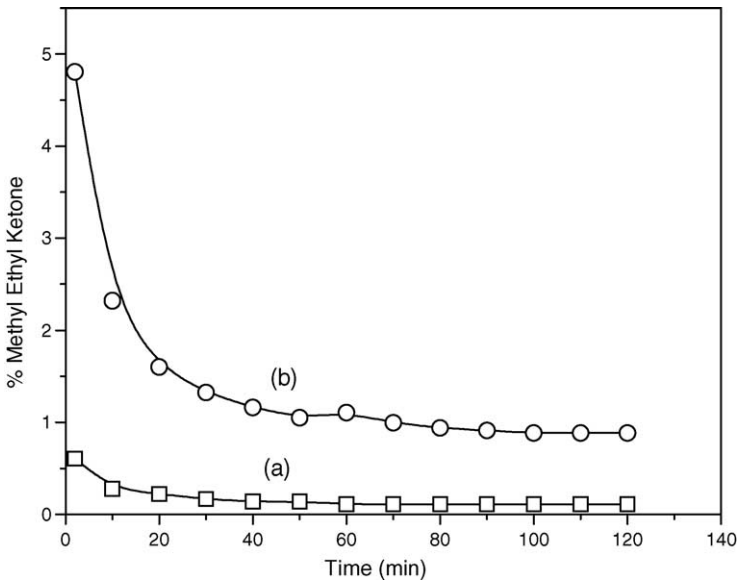

Fig. 4. Catalytic activity of $AgCaCdMg_2(PO_4)_3$ (a) and $AgCd_2Mg_2(PO_4)_3$ (b) in the absence of oxygen in the reaction mixture. $T_{reaction}$: 225 °C, $P_{butan\text{-}2\text{-}ol}$: 12.5×10^3 Pa, D_t: 60 mL min^{-1}.

3.3. Catalytic activity

The results of the experiments performed at 225 °C in the absence of oxygen are reported in Fig. 4 which shows that both samples exhibit poor efficiency; albeit, the dehydrogenation activity of $AgCd_2Mg_2(PO_4)_3$ is superior to that of $AgCaCdMg_2(PO_4)_3$. No dehydration activity was observed in these experimental conditions.

The substitution of N_2 by air in the reaction mixture produces an improvement of the catalyst performances. Fig. 5 displays the evolution of the dehydrogenation activity of $AgCaCdMg_2(PO_4)_3$ versus the reaction temperature. The production of methyl ethyl ketone which is the only product of the reaction increases with time on stream and temperature and reaches a stationary state after 1 h. No dehydration activity is observed, whereas the nasicon-type phosphates exhibit an important dehydration activity. This feature probably results from the differences between the alluaudite and nasicon acid–base properties.

We have followed the evolution of the production of methyl ethyl ketone for $AgCd_2Mg_2(PO_4)_3$ versus temperature and time on stream (Fig. 6). At all temperatures, the activity decreases slightly at the beginning of the experiment, reaches a maximum after 125 min, then decreases slowly. It is important to note the different behavior of these compounds, when we compare their activity at stationary state and different reaction temperatures (Fig. 7). According to this diagram, $AgCaCdMg_2(PO_4)_3$ is much more efficient than $AgCdMg_2(PO_4)_3$.

The catalytic behaviour of the alluaudite-type materials can be compared with that of nasicon-type catalysts which were previously investigated in the same probe reaction. Their activity might be attributed to the reduction ability of the Ag^+ ions located in the channels of the alluaudite structure and the formation of Ag^0 clusters. These aggregates of silver react with the oxygen of the reaction mixture, in order to form (Ag_xO_y) species which constitute the active sites. Analogous reduction and

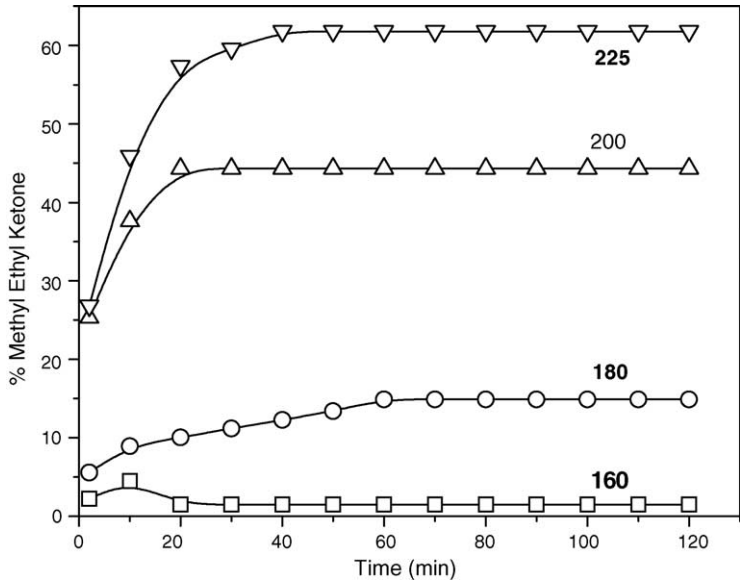

Fig. 5. Catalytic activity of $AgCaCdMg_2(PO_4)_3$ vs. reaction time, in the presence of oxygen in the reaction mixture. $P_{butan\text{-}2\text{-}ol}$: 12.5×10^3 Pa, D_t: 60 mL min^{-1}.

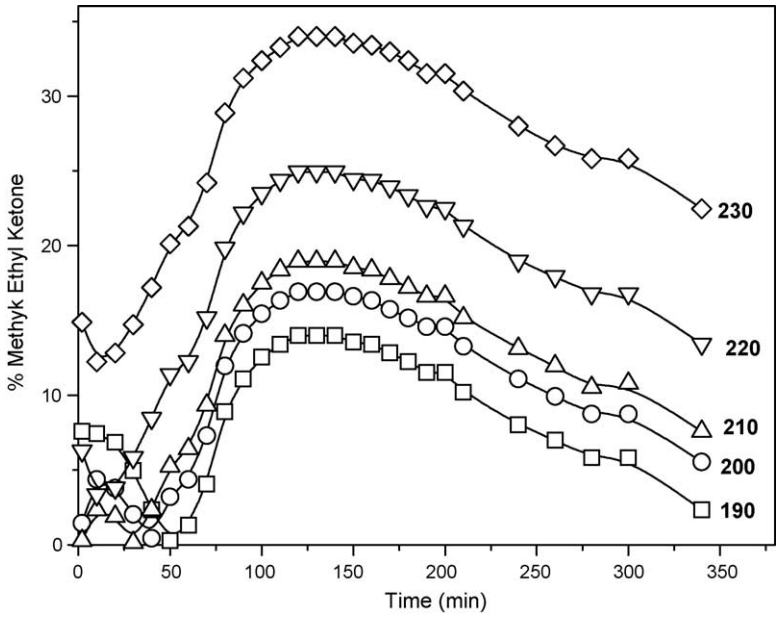

Fig. 6. Catalytic activity of $AgCd_2Mg_2(PO_4)_3$ vs. reaction time, in the presence of oxygen in the reaction mixture. $P_{butan\text{-}2\text{-}ol}$: 12.5×10^3 Pa, D_t: 60 mL min^{-1}.

oxidation processes were observed with the nasicon-type phosphates $AgZr_2(PO_4)_3$, $AgHf_2(PO_4)_3$ and $AgTh_2(PO_4)_3$ using the same probe reaction. The extent of this reduction obviously depends on the structural features of these phosphates [4,6]. This redox model explains the differences of behavior observed for both catalysts investigated in the present study.

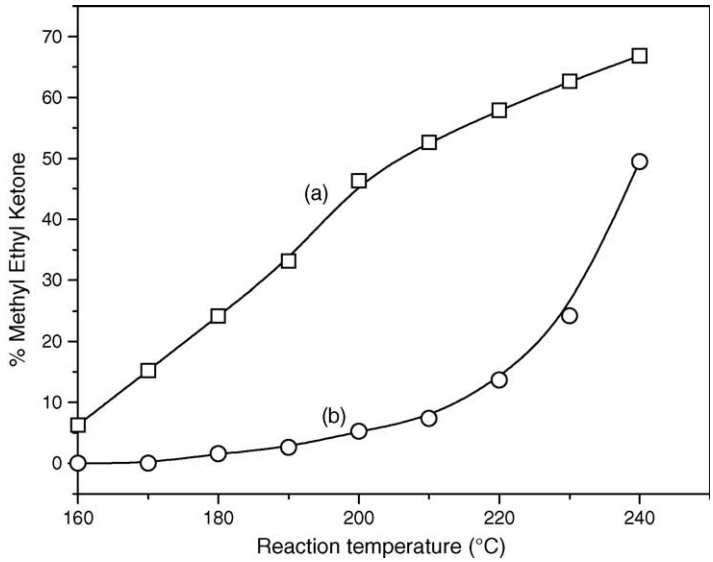

Fig. 7. Catalytic activity of $AgCaCdMg_2(PO_4)_3$ (a) and $AgCd_2Mg_2(PO_4)_3$ (b) vs. reaction temperature, in the presence of oxygen in the reaction mixture. $P_{butan\text{-}2\text{-}ol}$: 12.5×10^3 Pa, D_t: 60 mL min^{-1}.

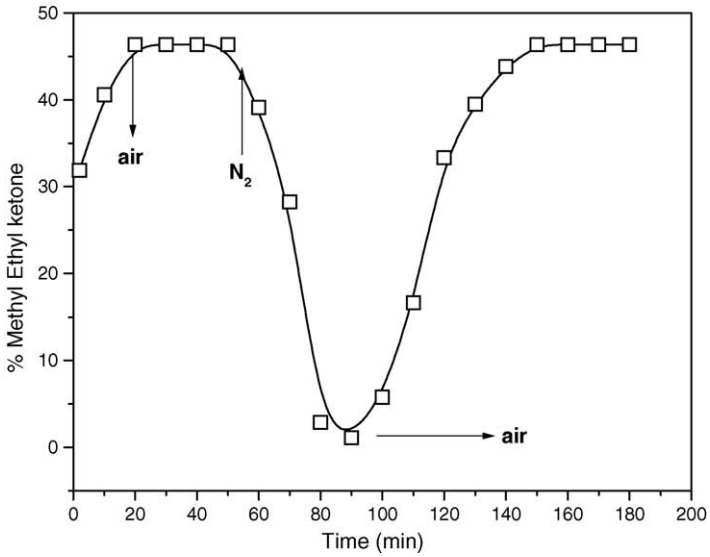

Fig. 8. Catalytic activity of $AgCaCdMg_2(PO_4)_3$ vs. reaction time, with alternations of the butan-2-ol + air and butan-2-ol + N_2 reaction mixtures. $P_{butan\text{-}2\text{-}ol}$: 12.5×10^3 Pa, D_t: 60 mL min^{-1}.

Complementary experiments were performed using a reaction mixture containing alternatively oxygen (Fig. 8). The experiments were undertaken in order to confirm the reversibility of the reduction process of Ag^+ ions. The replacement of air and butan-2-ol mixture by N_2 and butan-2-ol induces a rapid decrease of the catalytic activity. Oxygen addition to the reaction mixture enhances the catalytic activity. This reversible behavior is similar to that observed with the nasicon-type silver phosphates, for which the reduction of Ag^+ to Ag^0 has been previously demonstrated [16]. The active centers are the (Ag_xO_y) species and reaction mechanism is most likely of Mars and van Krevelen type.

4. Conclusion

The catalysts $AgCaCdMg_2(PO_4)_3$ and $AgCd_2Mg_2(PO_4)_3$, with the alluaudite-type structure, exhibit similar properties to those of nasicon-type phosphates. The promising catalytic results presented in this paper might probably be attributed to the extreme flexibility of the structure. Moreover, the nasicon-type compounds show essentially acidic properties, while the alluaudite-type phosphates could present acid or basic properties, depending on the nature of the cations introduced in the phosphate framework.

Acknowledgements

Many thanks are due to an anonymous reviewer, for his constructive comments. F. Hatert acknowledges the F.N.R.S. (Belgium) for a position of ''Chargé de Recherches'', as well as for grants # 1.5.112.02 and # 1.5.113.05.

References

[1] J.C. Védrine, Phosphorus Res. Bull. 10 (1999) 37.
[2] J.B. Moffat, Catal. Rev. Sci. Eng. 18 (1978) 199.
[3] A. Serghini, M. Kacimi, R. Brochu, M. Ziyad, J. Chim. Phys. 85 (4) (1988) 499.
[4] Y. Brik, M. Kacimi, F. Bozon-Verduraz, M. Ziyad, Micropor. Mesopor. Mater. 43 (1) (2001) 103.
[5] S. Arsalane, M. Kacimi, M. Ziyad, G. Coudurier, J.C. Védrine, Appl. Catal. 114 (1994) 243.
[6] M. Ziyad, S. Arsalane, M. Kacimi, G. Coudurier, J.-M. Millet, J.C. Vedrine, Appl. Catal. 147 (1996) 363.
[7] A. Benarafa, M. Kacimi, S. Gharbage, J.-M. Millet, M. Ziyad, Mater. Res. Bull. 35 (2000) 2047.
[8] A. Benarafa, M. Kacimi, G. Coudurier, M. Ziyad, Appl. Catal. A 196 (2000) 25.
[9] P.B. Moore, Am. Miner. 56 (1971) 1955.
[10] E.R. Losilla, S. Bruque, M.A.G. Aranda, L. Moreno-Real, E. Morin, M. Quarton, Solid State Ion. 112 (1998) 53.
[11] T.E. Warner, M. Milius, J. Maier, J. Solid State Chem. 106 (1993) 301.
[12] T.E. Warner, J. Maier, Mater. Sci. Eng. B 23 (1994) 88.
[13] N. Chouaibi, A. Daidouh, C. Pico, A. Santrich, M.L. Veiga, J. Solid State Chem. 159 (2001) 46.
[14] D. Kulkarni, I.E. Wachs, Appl. Catal. A: Gen. 6162 (2002) 1.
[15] D. Antenucci, A.M. Fransolet, G. Miehe, P. Tarte, Eur. J. Miner. 7 (1995) 175.
[16] S. Arsalane, K. Oulad Haj Ali, M. Kacimi, R. Brochu, M. Ziyad, J. Chim. Phys. 92 (1995) 1428.
[17] O.V. Yakubovich, M.A. Simonov, Y.K. Egorov-Tismenko, N.V. Belov, Sov. Phys. Dokl. 22 (1977) 550.
[18] D. Antenucci, Ph.D. Thesis, University of Liège, 1992, 259 pp.
[19] F. Leroux, A. Mar, C. Payen, D. Guyomar, A. Verbaere, Y. Piffard, J. Solid State Chem. 115 (1995) 240.
[20] F. Leroux, A. Mar, D. Guyomar, Y. Piffard, J. Solid State Chem. 117 (1995) 206.
[21] K.H. Lii, J. Ye, J. Solid State Chem. 131 (1997) 131.
[22] M.B. Korzenski, G.L. Schimek, J.W. Kolis, G.J. Long, J. Solid State Chem. 139 (1998) 152.
[23] F. Hatert, P. Keller, F. Lissner, D. Antenucci, A.-M. Fransolet, Eur. J. Miner. 12 (2000) 847.
[24] F. Hatert, D. Antenucci, A.-M. Fransolet, M. Liégeois-Duyckaerts, J. Solid State Chem. 163 (2002) 194.
[25] A. Guesmi, A. Driss, Acta Cryst. C58 (2002) i16.
[26] A. Daidouh, C. Durio, C. Pico, M.L. Veiga, N. Chouaibi, A. Ouassini, Solid State Sci. 4 (2002) 541.
[27] R. Ben Smail, T. Jouini, Acta Cryst. C58 (2002) i61.
[28] A. Brahim, H. Amor, Acta Cryst. E59 (2003) i77.
[29] F. Hatert, R.P. Hermann, G.J. Long, A.-M. Fransolet, F. Grandjean, Am. Miner. 88 (2003) 211.
[30] M. Hidouri, B. Lajmi, A. Driss, M. Ben Amara, Acta Cryst. E59 (2003) i7.
[31] C.W. Burnham, LCLSQ version 8.4, least-squares refinement of crystallographic lattice parameters, Department of Earth and Planetary Science, Harvard University, 1991.
[32] R.A. Young, A.C. Larson, C.O. Paiva-Santos, User's guide to program DBWS-9807 for Rietveld analysis of X-ray and neutron powder diffraction patterns, School of Physics, Georgia Institute of Technology, Atlanta, 1998, 56 pp.
[33] R.D. Shannon, Acta Cryst. A32 (1976) 751.
[34] A. Rulmont, R. Cahay, M. Liégeois-Duyckaerts, P. Tarte, Eur. J. Solid State Inorg. Chem. 28 (1991) 207.
[35] D. Antenucci, G. Miehe, P. Tarte, W.W. Schmahl, A.-M. Fransolet, Eur. J. Miner. 5 (1993) 207.